J Supercond Nov Magn (2015) 28:1261–1266
DOI 10.1007/s10948-014-2901-9

ORIGINAL PAPER

Monotonic Doping-Dependence in the Anisotropy of the Drude Weight and Scattering Rate of Detwinned $Ba(Fe_{1-x}Co_x)_2As_2$ Established from the Optical Conductivity

A. Dusza · A. Lucarelli · J.-H. Chu · I. R. Fisher · L. Degiorgi

Received: 31 July 2014 / Accepted: 5 November 2014 / Published online: 10 December 2014

Abstract We investigate the anisotropic metallic response in the optical conductivity of fully detwinned $Ba(Fe_{1-x}\ Co_x)_2As_2$ in their underdoped regime. We estimate the Drude weight and the scattering rates of the itinerant charge carriers across the structural (at T_s) and magnetic (at T_N) phase transition. Our findings support a monotonic doping dependence of the anisotropy of both parameters determining the transport properties, opposite to the non-monotonic anisotropy of the dc resistivity between the crystallographic axes. The capability of optical methods to address a broad energy interval extending far away from the Fermi level allows emphasizing the prominent role of the electronic structure rather than the impurity scattering when establishing a direct connection with the long-range ferro-orbital and antiferromagnetic orders.

Keywords Iron-pnictide superconductors · Optical properties

A. Dusza · A. Lucarelli · L. Degiorgi (✉)
Laboratorium für Festkörperphysik, ETH - Zürich,
8093 Zürich, Switzerland
e-mail: degiorgi@solid.phys.ethz.ch

J.-H. Chu · I. R. Fisher
Geballe Laboratory for Advanced Materials
and Department of Applied Physics, Stanford University,
Stanford, CA 94305-4045, USA

J.-H. Chu · I. R. Fisher
Stanford Institute for Materials and Energy Sciences,
SLAC National Accelerator Laboratory,
2575 Sand Hill Road, Menlo Park, CA 94025, USA

The title compounds provide the most recent arena in order to study the impact on several physical quantities of an electronic nematic phase, which occurs when the electronic system breaks a discrete rotational symmetry of the crystal lattice without altering the translational symmetry. In the title compounds, the structural tetragonal-to-orthorhombic phase transition breaks the fourfold rotational symmetry of the tetragonal phase. There are several experimental evidences [1] of nematicity in the iron-pnictides, which affects a vast range of their generic phase diagram and extends up to optimally doped compositions, thus implying some relationship with superconductivity at high temperature, as well.

Since the ferro-elastic transition induces the formation of dense structural twins in order to minimize the elastic energy, applying large magnetic fields or uniaxial pressure (strain) turns out to be essential in order to overrule the overcasting effect of randomly oriented domains when addressing the in-plane anisotropy of the orthorhombic phase [1]. Most experiments were performed with specimens constantly held under uniaxial stress in order to fully detwinned the crystals. Here, we shall briefly review the dc transport results, which serve the purpose to set the stage for the motivation of the present work. The resistivity on as-grown crystals along the shorter orthorhombic ferromagnetic b-axis (ρ_b) is larger than along the elongated orthorhombic antiferromagnetic a-axis (ρ_a) [2]. Such a counterintuitive behavior in the dc resistivity is accompanied by an astonishing non-monotonic anisotropy of the transport properties (i.e., ρ_b/ρ_a) as a function of doping in the $Ba(Fe_{1-x}Co_x)_2As_2$ series [2, 3]. Moreover, the most recent transport investigation with tunable in-plane uniaxial strain via a piezo-stack further reveals a divergent, substantial nematic susceptibility, indicating an electronic nematic quantum phase [3].

The non-monotonic dc anisotropy has been also confirmed in the underdoped regime of $Ba(Fe_{1-x}Ni_x)_2As_2$ and $Ba(Fe_{1-x}Cu_x)_2As_2$ [4], pointing out its generic nature and thus posing the pertinent question about its origin. Such a non-monotonic dc anisotropy is even more puzzling when compared to the monotonic doping-dependence of the orthorhombicity $(a - b)/(a + b)$ (a and b are the lattice constants of the respective axes) [5].

The dc transport properties are notoriously determined by the physics at energies close to the Fermi level, therefore raising the issue to which extent in energy scales and how deep in the electronic structure one can directly image the impact of the nematic phase. There is the need to clarify, whether and how the non-monotonic anisotropy of the dc transport is possibly reflected in the effective metallic contribution of the charge dynamics. Here, we exploit the capability of optical methods to cover a broad spectral range, enabling us to extract both parameters determining the dc properties, as the plasma frequency (related to the Drude weight) and the scattering rate of the itinerant charge carriers. We can establish a robust link to the dc transport properties from the perspective of a broad spectral range (addressing the whole conduction bands) and investigate the evolution of these parameters within the underdoped regime of the phase diagram of $Ba(Fe_{1-x}Co_x)_2As_2$.

Single crystals of $Ba(Fe_{1-x}Co_x)_2As_2$ with $x = 0$, 2.5, and 4.5 % were grown using a self-flux method [2]. Crystals were cut into a square shape, approximately 2 mm on the side, oriented such that below T_s the orthorhombic a/b axes are parallel to the sides of the square [2]. Single-domain specimens, revealing the intrinsic anisotropy of the orthorhombic phase, are achieved by exerting constant uniaxial pressure on their lateral side. To that goal, we further developed the basic cantilever concept originally designed for transport measurements [1].

The reflectivity ($R(\omega)$) at room temperature was first collected from different spectrometers such as the Bruker IFS48 for the mid-infrared (MIR, 500–4000 cm^{-1}) and near-infrared (NIR, 4000–7000 cm^{-1}) measurements and a PerkinElmer Lambda 950 capable to measure absolute reflectivity from NIR up to the ultra-violet (UV) range, i.e., 3200–4.8 $\times$ 10^4 cm^{-1}. The specimen within the detwinning pressure device (i.e., mechanical clamp) was then placed inside our cryostat and finely aligned within the optical path of the Fourier transform infrared Bruker Vertex 80v interferometer by using a micrometer. This way, we could perform optical measurements of $R(\omega)$ at different temperatures in the spectral range from the far-infrared (FIR, $\omega <$ 400 cm^{-1}) up to the MIR, i.e., between 30 and 6000 cm^{-1}. Light in all spectrometers was polarized along the a and b axes of the detwinned samples. The real part $\sigma_1(\omega)$ of the optical conductivity was obtained via the Kramers-Kronig transformation of $R(\omega)$ by applying suitable extrapolations at low and high frequencies. For the $\omega \rightarrow 0$ extrapolation, we made use of the Hagen-Rubens (HR) formula $\left(R(\omega) = 1 - 2\sqrt{\frac{\omega}{\sigma_{dc}}}\right)$, inserting the dc conductivity values (σ_{dc}) from [2], while above the upper frequency limit $R(\omega) \sim \omega^{-s}$ ($2 \leqslant s \leqslant 4$) [13]. The merging of the measured data with the HR extrapolation was performed in the energy interval between 30 and 70 cm^{-1}. The latter energy interval corresponds to the lowest trustable FIR range, depending from the surface quality of the specimen. Details pertaining to the experimental set-up, techniques, and procedures can be obtained by consulting [6].

While a thorough display of the experimental optical findings is given in [6], we summarize in Fig. 1 some selected and representative data about the real part ($\sigma_1(\omega)$) of the optical conductivity with light polarized along both orthorhombic axes and at characteristic temperatures above and below the respective transitions at T_s and T_N of three Co-dopings, spanning the generic underdoped regime of the 122 family of iron pnictides. We specifically emphasize here the FIR and MIR spectral range, where the clearest evidence for the anisotropic optical response may be recognized. Nonetheless, the inset in panel (a) shows the spectra up to the NIR frequency range for $x = 0$. Above 5000 cm^{-1}, the spectra at all T and for every doping fully coincide. The strong absorption peak dominating $\sigma_1(\omega)$ at about 5000 cm^{-1} develops into a pronounced shoulder on its MIR frequency tail at about 1500 cm^{-1} for $x = 0$. This latter MIR-band in $\sigma_1(\omega)$ shows a strong polarization dependence, as highlighted in the main panels of Fig. 1a–c. Interestingly enough, for increasing doping, the maximum of the MIR-peak shifts to lower frequencies indicating that this absorption feature is significantly affected by the doping. This excitation turns out to be very much related to the onset of the SDW-like state in the orthorhombic phase and its polarization dependence was previously identified as the most evident signature of the stress-induced optical anisotropy [6–9]. $Ab-initio$ calculations based on DFT as well as dynamical mean-field theory (DMFT) [6, 10] fairly reproduce the anisotropic MIR-feature and account for it as a fingerprint of the stripe-like magnetic ordering in the orthorhombic state, which was also shown to correspond to the energy-minimum configuration within LAPW calculations [10]. For frequencies going towards zero (i.e., into the FIR spectral range), one can observe a narrow effective metallic contribution for both polarization directions. It is an interesting experimental observation that the metallic part of $\sigma_1(\omega)$ along the a-axis broadens while along the b-axis, $\sigma_1(\omega)$ more strongly narrows with decreasing T into the orthorhombic phase [6].

Before going any further, it is worth mentioning that in a previous work, focusing the attention on the distribution of the integrated spectral weight ($SW = \int_0^{\omega_c} \sigma_1(\omega) d\omega$, ω_c being an appropriate cut-off energy) within the

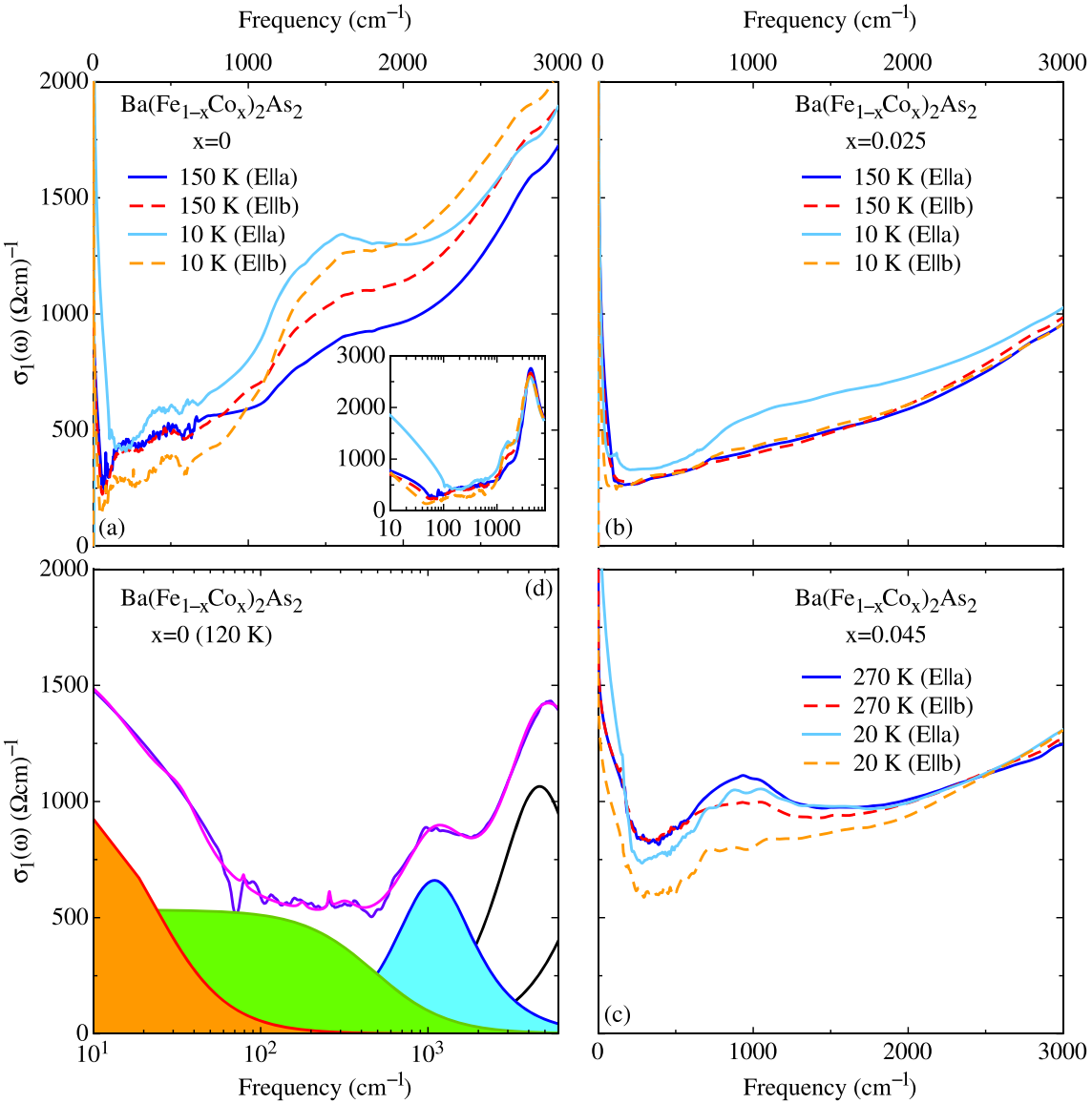

Fig. 1 a–c Real part $\sigma_1(\omega)$ of the optical conductivity of Ba(Fe$_{1-x}$Co$_x$)$_2$As$_2$ for $x = 0$, 2.5, and 4.5 % in the FIR to MIR spectral range at selected temperatures above and below T_s and for both polarization directions [6]. The *inset* of panel (**a**) displays $\sigma_1(\omega)$ for $x = 0$ over the whole spectral range extending up to the NIR energy interval (please note the logarithmic energy scale). Panel (**d**) reproduces the data for $x = 0$ at 120 K and emphasizes the components of the Drude-Lorentz fit procedure (see text) and the good quality achieved in the data-fit [6] (please note the logarithmic energy scale). For clarity, we omit to display the tiny, sharp phonon modes, which, however, are negligible to the present discussion (*color online*)

orthorhombic phase [11], we clearly identified $\omega_c \sim 10^4$ cm^{-1} as energy scale marking the recovery at all temperatures of the total *SW* of the paramagnetic state. Furthermore, the coherent metallic part was found to mainly develop along the orthorhombic *a*-axis, while the SDW state leading to the depletion of *SW* and the opening of the pseudogap-like excitation in the MIR range affects principally the orthorhombic *b*-axis [11].

In order to phenomenologically describe the optical response, we apply the well-established Drude-Lorentz approach. Figure 1d presents all fit components for $x = 0$ at 120 K, acting here as a representative example. We ascribe two Drude contributions (narrow and broad) to the effective metallic part of $\sigma_1(\omega)$ and a series of Lorentz harmonic oscillators (h.o.) for all excitations (phononic and electronic) at finite frequencies. The use of two Drude components in the fit procedure mimics the multi-band scenario and implies the existence of two electronic subsystems as revealed for an ample range of iron-pnictide compounds [12].

The narrow Drude term is relevant at very low frequencies and it is obviously tied to the necessary HR

extrapolation of $R(\omega)$ for $\omega \rightarrow 0$. The broad one acts as a background of $\sigma_1(\omega)$ and dominates the optical conductivity up to the MIR energy interval. Both Drude terms contribute to the total dc conductivity (see below). Besides the Drude contributions, we consider one broad h.o. for the temperature-dependent MIR-band (blue area in Fig. 1d) and three more broad h.o.'s (not shown, see Fig. 5 in [6] for details) for the strong absorptions featuring the broad peak centered at about 5000 cm^{-1} in $\sigma_1(\omega)$. We favor a fitting procedure for all dopings, which keeps the type and number of components identical (Fig. 1d) above and below T_s for both polarization directions. The fit constraints are such that the measured $R(\omega)$ and $\sigma_1(\omega)$ are simultaneously reproduced by the identical set of fit-components as well as fit-parameters for both quantities [6]. The upper boundary for the temperature dependence of the optical conductivity is found to be close to the NIR peak in $\sigma_1(\omega)$ at about 5000 cm^{-1} for all dopings. It turns out that the whole electronic anisotropy is exhausted within the measured spectral range. The overall good fit quality (e.g., Fig. 1d) makes us confident that our fit-procedure is a valuable route in order to identify meaningful and consistent trends in relevant physical parameters.

We now turn our attention to the distribution of the metallic Drude spectral weight and to the scattering rates of the itinerant charge carriers. The former quantity is given by the sum of the spectral weight encountered in both broad and narrow Drude components (i.e., orange

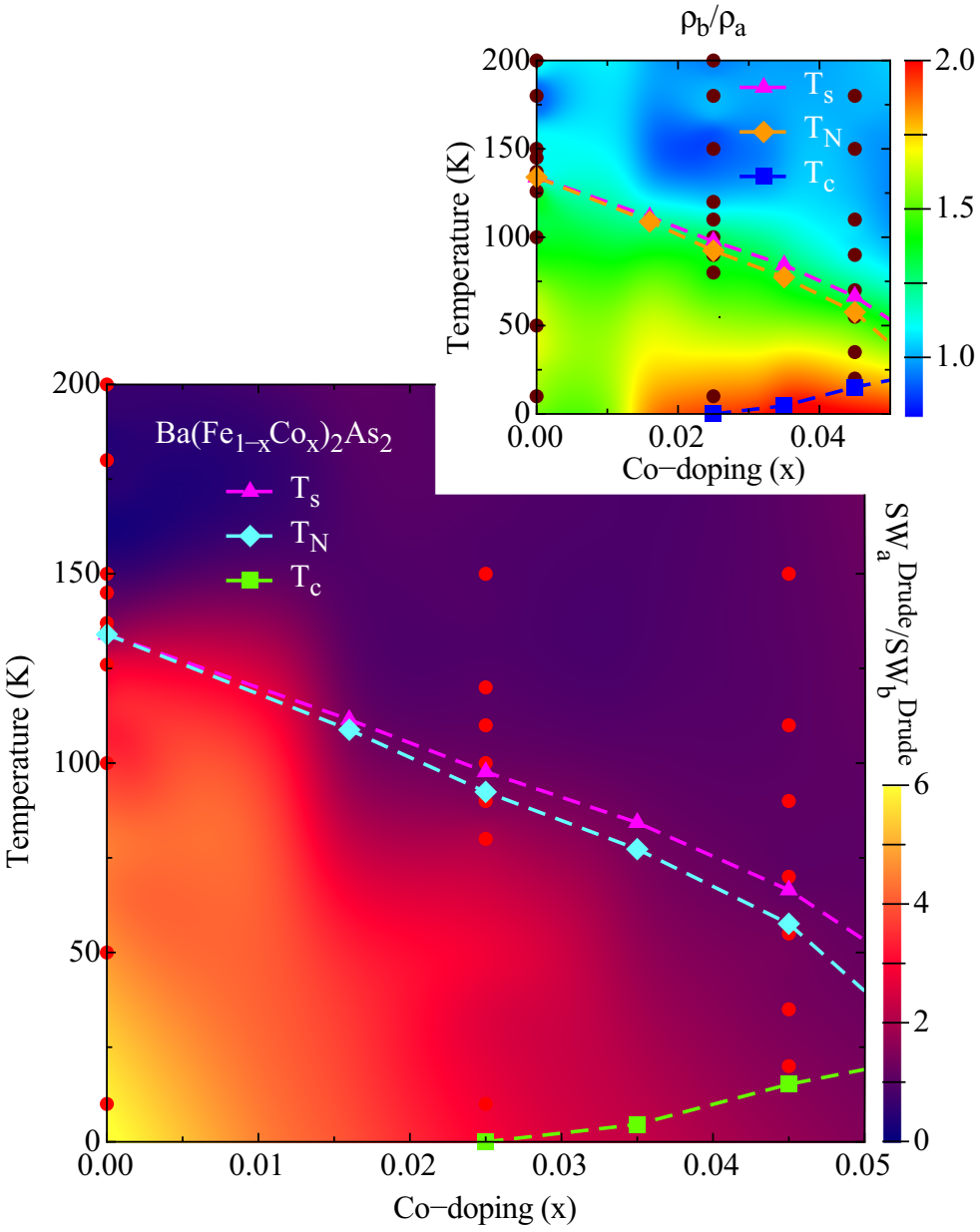

Fig. 2 Temperature and doping dependence of the ratio of the total Drude weight between the a and b axis ($SW_a^{Drude}/SW_b^{Drude}$), emphasizing the underdoped regime of $Ba(Fe_{1-x}Co_x)_2As_2$ [1]. The *upper-right panel* shows the calculated dc anisotropy ρ_b/ρ_a from our fit parameters (see text). The *dots mark* the combinations of doping and temperature for which data were effectively collected. Both *color panels* are then obtained through an interpolation of the data points (*color online*)

and green area in Fig. 1d), which is basically equal to $SW^{Drude} \sim \omega_{pN}^2 + \omega_{pB}^2$, $\omega_{pN/B}$ being the plasma frequency of the narrow and broad Drude resonance, respectively. The scattering rate ($\Gamma_{N/B}$) corresponds to the width at half maximum of the Drude terms themselves. Here, we are particularly eager to disentangle the anisotropy as a function of doping and across the structural and magnetic phase transitions of both parameters determining the *dc* transport properties. We rely on the fit parameters reported in [6]. Figure 2 displays the ratio between the total Drude weight along the *a*- and *b*-axis with respect to the phase diagram of $Ba(Fe_{1-x}Co_x)_2As_2$ in the underdoped regime [1]. In a

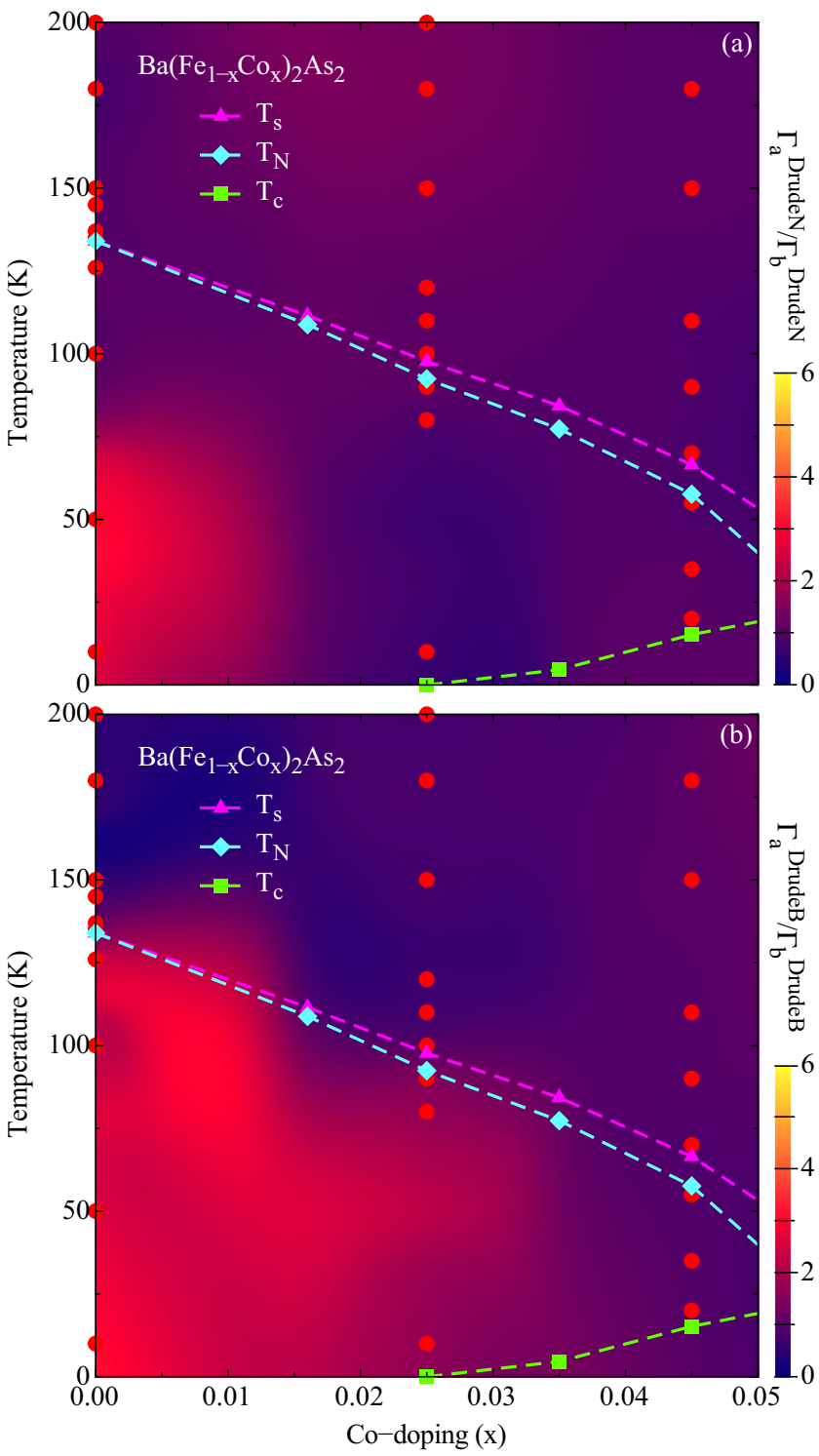

Fig. 3 **a–b** Similar to Fig. 2, we show the temperature and doping dependence of the ratio of the scattering rates (**a** narrow (N) and **b** broad (B) Drude term) between the *a* and *b* axis ($\Gamma_a^{DrudeN}/\Gamma_b^{DrudeN}$ and $\Gamma_a^{DrudeB}/\Gamma_b^{DrudeB}$), emphasizing the underdoped regime of $Ba(Fe_{1-x}Co_x)_2As_2$ [1] (*color online*)

similar fashion, Fig. 3 emphasizes the anisotropy of the scattering rates between the a- and b-axes for both narrow and broad Drude components. For temperatures below T_N, the topology of the reconstructed Fermi surface, combined with the distinct behavior of the scattering rates, determines the anisotropy of the low-frequency optical response. We observe an enhancement as well as a depletion or reduction of both parameters associated to the itinerant charge carriers along the orthorhombic antiferromagnetic a-axis and ferromagnetic b-axis, respectively. The temperature dependence of the scattering rates and their anisotropy are moreover consistent with the well-established magnetic order in these materials below T_N [1, 6]. The anisotropy of the optical conductivity extends to high frequencies in the mid- and near-infrared regions. The reshuffling of SW at low frequencies ultimately gives rise to the narrow metallic components and the MIR feature in $\sigma_1(\omega)$ at $T < T_s$ (Fig. 1).

Contrary to the non-monotonic dc anisotropy, the Drude weight as well as the scattering rates clearly display a monotonic doping dependence. As we have already anticipated in [6], the Drude weight anisotropy outweighs the equally important anisotropy of the scattering rates, guaranteeing nonetheless a great agreement between the dc conductivity, as evinced from the $\omega \rightarrow 0$ limit of $\sigma_1(\omega)$ within our Drude-Lorentz model, and the dc transport data and their non-monotonic behavior upon doping [2]. This is explicitly shown in the upper-right panel of Fig. 2, reproducing ρ_b/ρ_a calculated from our Drude fit parameters (i.e., $\rho_i = (\omega_{pN}^2/(4\pi\Gamma_N) + \omega_{pB}^2/(4\pi\Gamma_B))^{-1}$, $i = a$ and b) [6], which also represents a robust self-consistency check of our phenomenological approach. The monotonic metallic spectral weight anisotropy thus follows very much the strength of the ferro-orbital and antiferromagnetic order parameter all the way to the zero doping. This is in clear contrast to the transport measurement, which is likely complicated and masked by the additional Dirac particles. Therefore, the physics behind the transport anisotropy might well not be related to impurity scattering, as claimed on various occasions, but primarily originates from the electronic structure itself. The different and puzzling behavior upon doping of the dc anisotropy might occur because of the multi-band nature of the title compounds. Since transport measurements are only sensitive to small energy scales close to the Fermi level, it is possible to get quite non-monotonic behavior of the transport anisotropy across the phase diagram depending on what the underlying bands are doing. Moreover, the non-monotonic resistivity anisotropy mainly appears in the antiferromagnetic state, where the Fermi surface (FS) has been severely reconstructed, and Lifshitz transitions may occur as a function of doping. Also, supported by magneto-transport data, it was suggested that the small in-plane dc anisotropy in the parent compound is mainly the consequence of the presence of an isotropic high mobility Dirac pocket, which is progressively suppressed upon doping [4]. In this sense, the resistivity anisotropy certainly does not have to track better avatars of the nematic order parameter as a function of doping and can be only revealed when the contribution due to the remaining anisotropic FS pockets dominates upon chemical substitution.

In conclusion, we chased the fingerprints of the electronic nematic phase on the effective metallic contribution in the charge dynamics of the title compounds. We consequently discussed the dichotomy between the monotonic anisotropy of the parameters determining transport and the non-monotonic one of the dc properties themselves with respect to the doping in iron-pnictides. This work finally emphasizes the importance of optical methods imaging a broad energy interval and therefore allowing a full view of the charge dynamics extending from the Fermi level, relevant for transport, deep into the electronic structure.

Acknowledgments The authors wish to thank P. Hirschfeld, K. Wu and C. Mirri for fruitful discussions. This work has been supported by the Swiss National Foundation for the Scientific Research. L.D. wishes to thank the hospitality of KITP at the University of California at Santa Barbara, where part of this paper has been written.

References

1. Fisher, I.A., Degiorgi, L., Shen, Z.X.: Rep Prog. Phys. **74**, 124506 (2011). and references therein
2. Chu, J.-H. et al.: Science **329**, 824 (2010)
3. Chu, J.-H. et al.: Science **337**, 710 (2012)
4. Kuo, H.-H. et al.: Phys. Rev. B **84**, 054540 (2011)
5. Prozorov, R. et al.: Phys. Rev. B **80**, 174517 (2009)
6. Dusza, A. et al.: New. J. Phys. **14**, 023020 (2012)
7. Dusza, A. et al.: Europhys. Lett. **93**, 37002 (2011)
8. Nakajima, M. et al.: PNAS **108**, 12238 (2011)
9. Nakajima, M. et al.: Phys. Rev. Lett. **109**, 217003 (2012)
10. Sanna, A. et al.: Phys. Rev. B **83**, 054502 (2011)
11. Dusza, A. et al.: J. Supercond. Nov. Magn. **26**, 2603 (2013)
12. Wu, D. et al.: Phys. Rev. B **81**(R), 100512 (2010)
13. Dressel, M., Grüner, G.: Electrodynamics of Solids. Cambridge University Press (2002)